CHAPTER 4

Synthesis of solketal from biowaste glycerol using sulfated Zr-Al based heterogeneous acid catalyst

4.1 Introduction

This chapter deals with the highly efficient and economically viable heterogeneous acid SO_4^{-2}/ZrO_2-Al_2O_3 catalyst, which was synthesized by a wetness impregnation process and its application in solketal synthesis. There are no reports available regarding the use of SO_4^{-2}/ZrO_2-Al_2O_3 catalyst in the glycerol conversion up to now. The current study aims to explore the effectiveness of SO_4^{-2}/ZrO_2-Al_2O_3 as a solid acid catalyst for the acetalization of glycerol to solketal synthesis. Various characterization techniques, including thermogravimetric analysis (TGA), X-ray diffraction (XRD), Fourier transform infrared spectroscopy (FT-IR), X-ray photoelectron spectroscopy (XPS), BET-surface area analysis, and NH_3-TPD analysis were used to characterize the physiochemical properties of the designed catalyst. The synthesized product was also analyzed by using GC-MS, ^1H, and ^{13}C NMR and FT-IR spectroscopy. The main objective of the present work was to synthesize a zirconia-alumina-based catalyst due to its cost-effective, robust acidic sites and conversion of glycerol to solketal at optimized reaction conditions through acetalization reaction. The incorporation of alumina in sulphonated zirconia increases the catalytic activity, good selectivity, easy separation, and stability of the catalyst, which helps in complete glycerol conversion and further utilization. In the acetalization reaction, the catalytic activity can be improved while time and temperature consumption are minimized. The environmental study of the designed catalysts was also explored to check the process's environmentally friendly path. Hence, based on the above-mentioned properties, the SO_4^{-2}/ZrO_2-Al_2O_3 catalyst was synthesized and investigated in glycerol acetalization.

4.2 Synthesis of SO_4^{-2}/ZrO_2-Al_2O_3 catalyst

A heterogeneous solid acid SO_4^{-2}/ZrO_2-Al_2O_3 catalyst utilized in the acetalization reaction of glycerol was synthesized by the wetness impregnation process. Initially, a

crucial amount of zirconyl nitrate and aluminum nitrate was dissolved in deionized water separately. The resulting solution was mixed and allowed to stir for 5-6 h at ambient conditions. Then, the temperature was raised to 50 ^{o}C with the addition of dropwise ammonium hydroxide solution to maintain the pH at 8-9. Furthermore, the precipitate mixture was also left for a better precipitate. The obtained precipitate was filtered and washed with deionized water several times to remove the impurities. The obtained white powder was kept in a hot air oven for 12-14 h at 383 K. Then calcined for 4 h at 800 ^{o}C to get the ZrO_2-Al_2O_3 (ZA). To increase the acidity of the synthesized catalyst, further modification was performed by incorporation of 0.5 M H_2SO_4 by wetness impregnation process for 4 h. Subsequently, it was dried and calcined in an air muffle furnace for 3 h at 550 ^{o}C. Finally, the obtained catalyst was crushed in a mortar pestle and kept in a desiccator and named SO_4^{-2}/ZrO_2-Al_2O_3 (SZA) for further application.

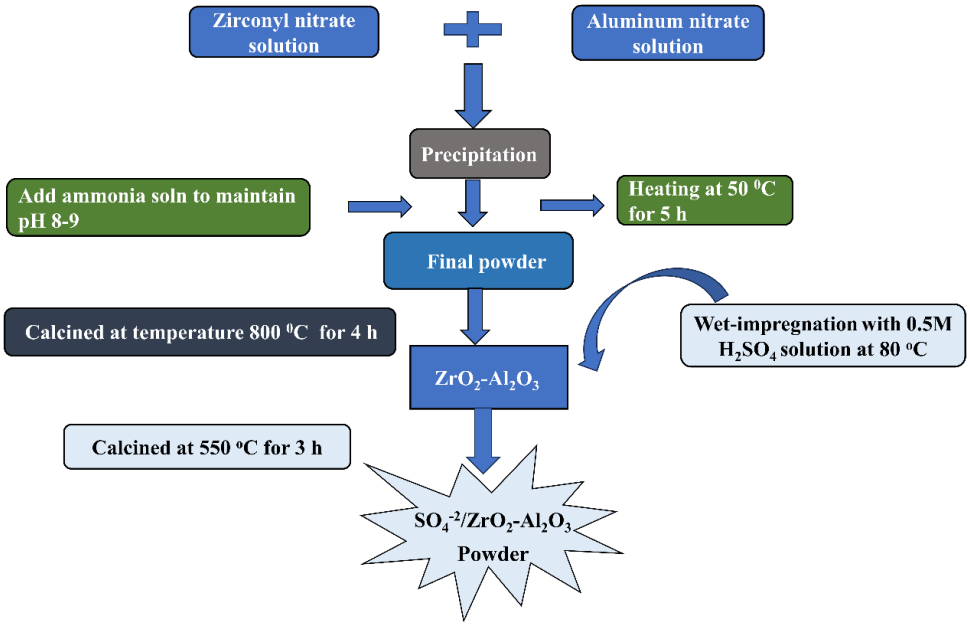

Scheme 4.1 Synthesis of SO_4^{-2}/ZrO_2-Al_2O_3 catalyst

4.3 Characterization of catalyst

4.3.1. TGA-DSC study

The synthesized uncalcined catalyst's thermal stability was analyzed using the TGA-DSC method. Figure 4.1 illustrates the plot of weight loss and heat flow versus temperature. It was found that the first weight loss was observed in the temperature range of 20-130 ^{o}C, corresponding to a broad endothermic peak attributed to the removal of physically bound water and gaseous molecules from the catalyst surface. A small endothermic peak was observed at 288.5 ^{o}C with a heat flow of 64.63 J/g, representing the weight loss, which might be due to the dehydroxylation of the hydroxyl group bound with the catalyst surface [86]. Two weight losses were detected above 650 ^{o}C, which could be attributed to the decomposition of the surface sulfate group. This examination reveals that the SZA catalyst surface contains two types of surface sulfate groups. When zirconia is mixed with another oxide, the thermal properties of the synthesized catalyst increase, as reported by various literature studies. Rajeswari et al. [87] explained that incorporating zirconia into the ceria oxide increases its thermal behavior compared to that of zirconium oxide alone. The same comparable peak type was observed in the case of the synthesized SZA catalyst, suggesting the decomposition of several surface sulfate groups observed at higher temperatures than SO_4^{-2}/ZrO_2. Hence, alumina acts as a promoter that increases the thermal stability and catalytic activity of the SO_4^{-2}/ZrO_2 catalyst, as revealed by the thermal study. Therefore, for maximum catalyst activity toward glycerol conversion, the catalyst's optimum calcination temperature was chosen between 500-600 ^{o}C.

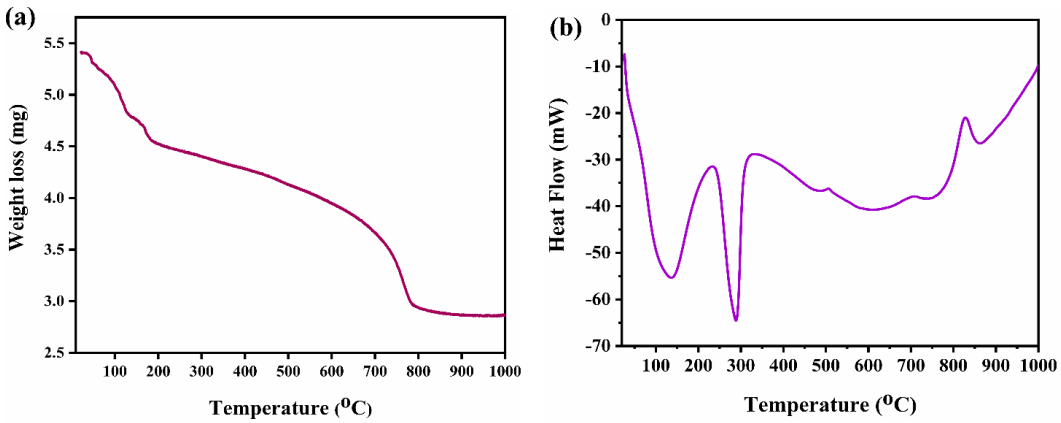

Figure 4.1 (a) TGA, (b) DSC plot of SZA catalyst

4.3.2. X-ray diffraction (XRD) analysis

XRD analysis was performed to examine the phases present in the crystal lattice. The diffraction of ZA and SZA is shown in Figure 4.2. The major diffraction peaks are positioned at 30.24° (101), 34.53° (002), 35.37° (110), 50.36° (112), 59.39° (103), and 60.32° (211). The peaks were matched with tetragonal ZrO_2 with JCPDS file no.- 881007. Broad peaks of tetragonal zirconia were observed, while peaks of alumina were not observed. This indicates that either alumina is homogeneously mixed with crystalline zirconia or is present in an amorphous state. Meanwhile, SO_4^{-2}/ZrO_2 shows both monoclinic and tetragonal phases. However, SO_4^{-2}/ZrO_2-Al_2O_3 exclusively exhibits only the tetragonal zirconia phase, and the inclusion of alumina in zirconia inhibits the transformation from the metastable tetragonal phase to the monoclinic phase. Therefore, the current study demonstrates that alumina serves as a structural stabilizer for zirconia, maintaining the tetragonal structure following sulphonation [88].

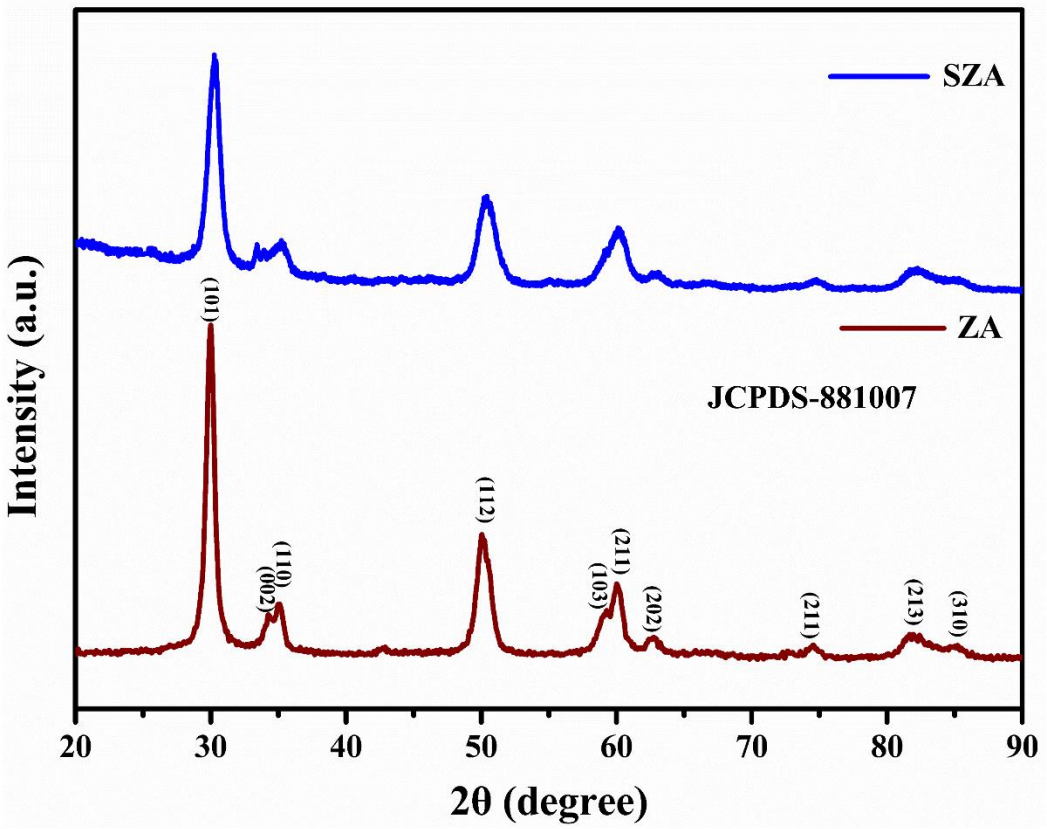

Figure 4.2 XRD of ZA and SZA catalyst

4.3.3. FT-IR analysis

The FT-IR spectroscopy explained the presence of functional groups on synthesized catalysts well. Figure 4.3 compares the freshly prepared SZA catalysts, reused SZA catalyst (after calcined at 550 ^{o}C), and reused SZA catalyst (without calcination). The absorption peaks observed between 410 and 820 cm^{-1} show the stretching bond of the M-O bond in the case of fresh SZA catalyst. After five catalytic cycles, the peaks become broader than the previous, while on calcination, the broadness of peaks slightly decreases. This might be due to the physical binding of water molecules on the catalyst's surface. The absorption peaks observed at 435 cm^{-1} and 680 cm^{-1} correspond to the stretching vibration of Zr-O and Al-O bonds, respectively [89]. The presence of a sulfate group on the surface is confirmed by the characteristic's peaks around 931 cm^{-1} and 1238 cm^{-1}. Further, the absorption peaks at ~ 930 and ~ 1250 cm^{-1} are attributed to the symmetric

and asymmetric stretching band of sulfate groups on the SZA surface [90]. Another band appeared at 1640 cm^{-1} and 3400 cm^{-1}, explaining the stretching and bending mode of vibration of the hydroxyl group, which could be due to the adsorption of water molecules on the catalyst surface.

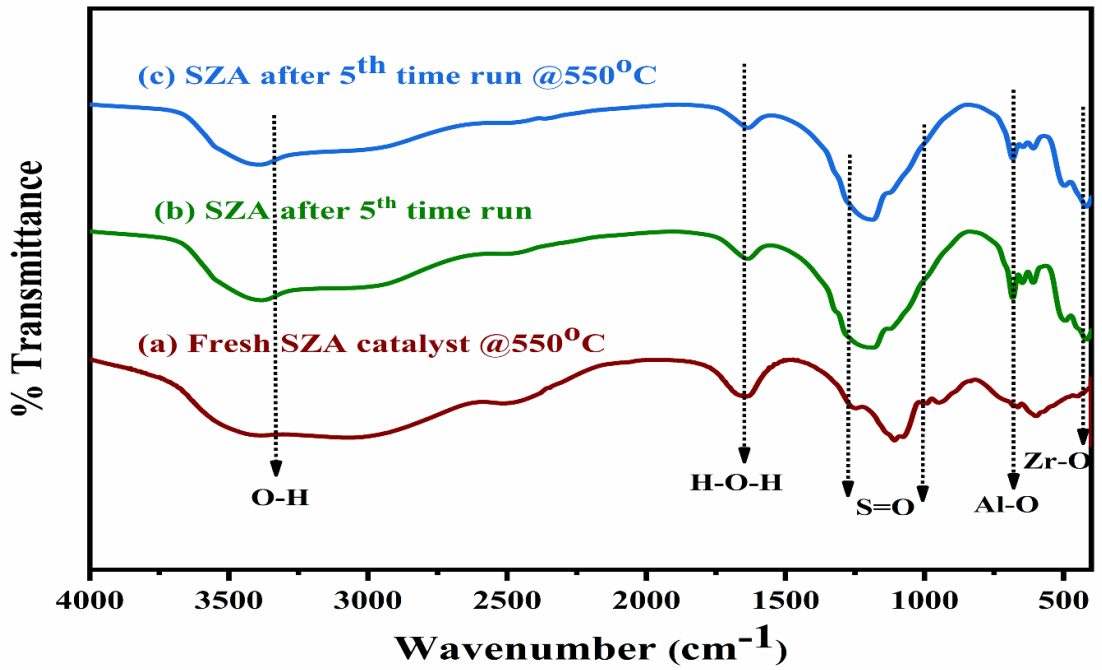

Figure 4.3. FT-IR spectra of fresh SZA catalyst calcined at 550 ºC, (b) SZA catalyst after five-time run without calcination, and (c) SZA catalyst after five-cycle uses in acetalization of glycerol calcined at 550 ºC.

4.3.4. BET-surface area analysis

The textural properties like surface area, pore volume, and pore diameter of synthesized ZA and SZA catalysts were determined by the BET-BJH method by using N_2-adsorption and desorption isotherm. Figures 4.4 (a) and (b) depict the isotherm of the catalyst, and the results obtained are shown in Table 2. The obtained adsorption and desorption isotherm shows the Type-IV hysteresis loop and confirms that the synthesized catalysts show a mesoporous nature [91]. The specific surface area of the ZA catalyst is 20.1 m^2/g, whereas the pore diameter and pore volume are 0.07cm^3/g and 13.8 nm. A change was

observed in the surface area of the SZA catalyst from 20.1 m^2/g to 2.9 m^2/g, and pore volume was observed at 0.07 cm^3/g to 0.01 cm^3/g. This could be due to the incorporation of the sulfate group in the ZA surface. As a result, the formation of Al and Zr sulfate at higher temperatures. It was evident that no XRD peaks were detected for the catalyst, likely because of its crystalline nature [92].

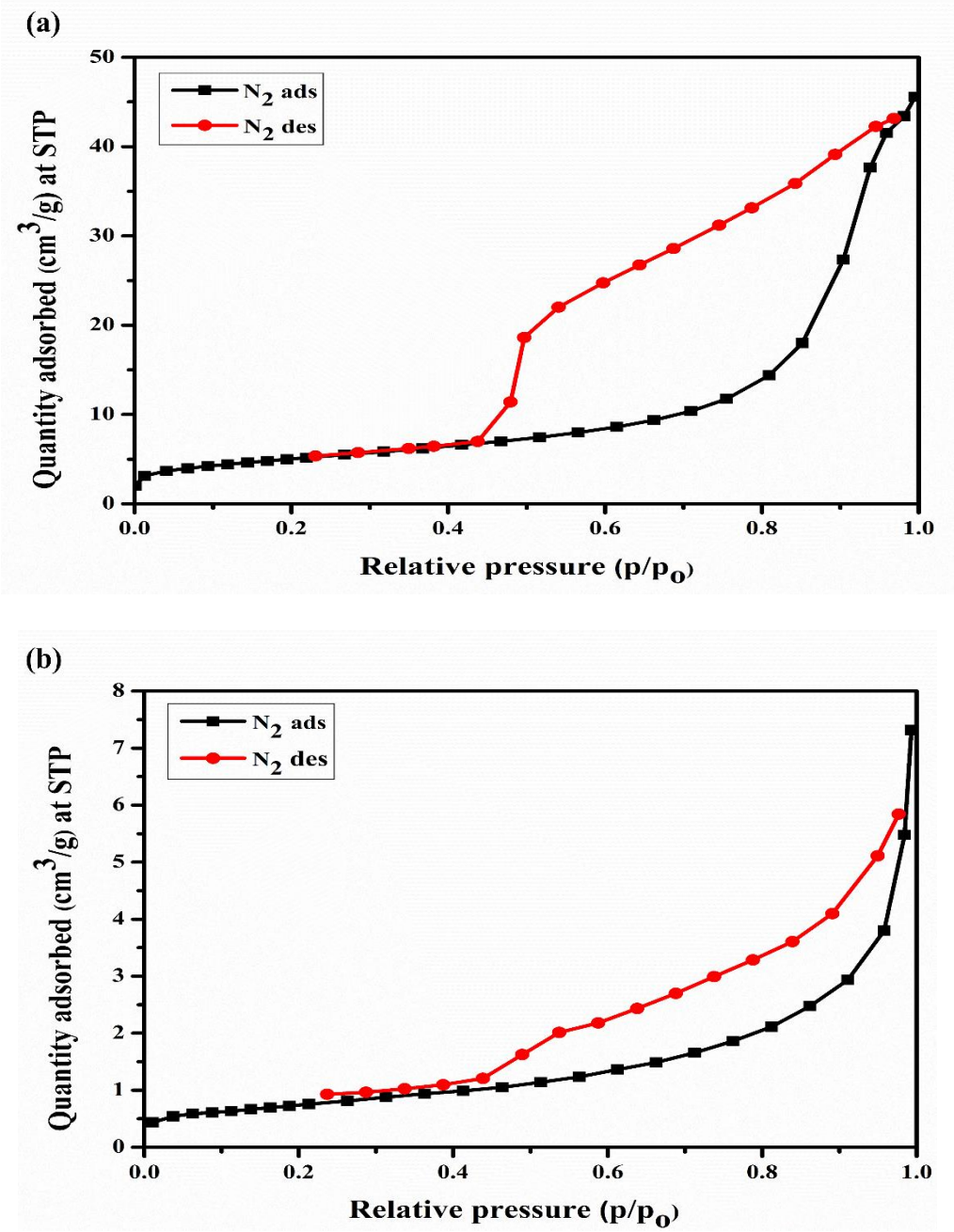

Figure 4.4 BET surface area of (a) ZA and (b) SZA catalyst

4.3.5. NH_3-TPD analysis

The acidic sites, strength, and amount of synthesized catalyst were calculated by using the NH3-Temeprature programmed desorption method. The desorption profile of ZA and SZA catalysts are illustrated in Figure 4.5. The desorption peak area and temperature were used to quantify the amount of acidic sites. The NH_3-TPD shows the two types of desorption peaks from 300 ^oC to 700 ^oC. The desorption peak present at lower temperature regions (<200 ^oC) corresponds to the weak acidic sites. The desorption peaks present at medium-temperature regions (200-400 ^oC) are attributed to the moderate acidic sites, whereas the peaks observed at high-temperature regions (>400 ^oC) represent the strongest acidic sites [93]. The synthesized ZA and SZA catalysts show two types of desorption peaks. The first one present at 200 ^oC might be due to the weak acidic sites, whereas the second desorption peaks obtained above 520 ^oC could be due to the stronger interaction of desorbed NH_3 molecules with both Lewis and Bronsted acidic sites. It was also found that the acidic strength of SZA increases with the incorporation of a sulfate group on Zirconia-alumina-based oxide [94]. Moreover, it was noted that the SZA catalyst demonstrates a greater acidic density than the ZA catalyst. The calculated acidic sites are shown in Table 4.1.

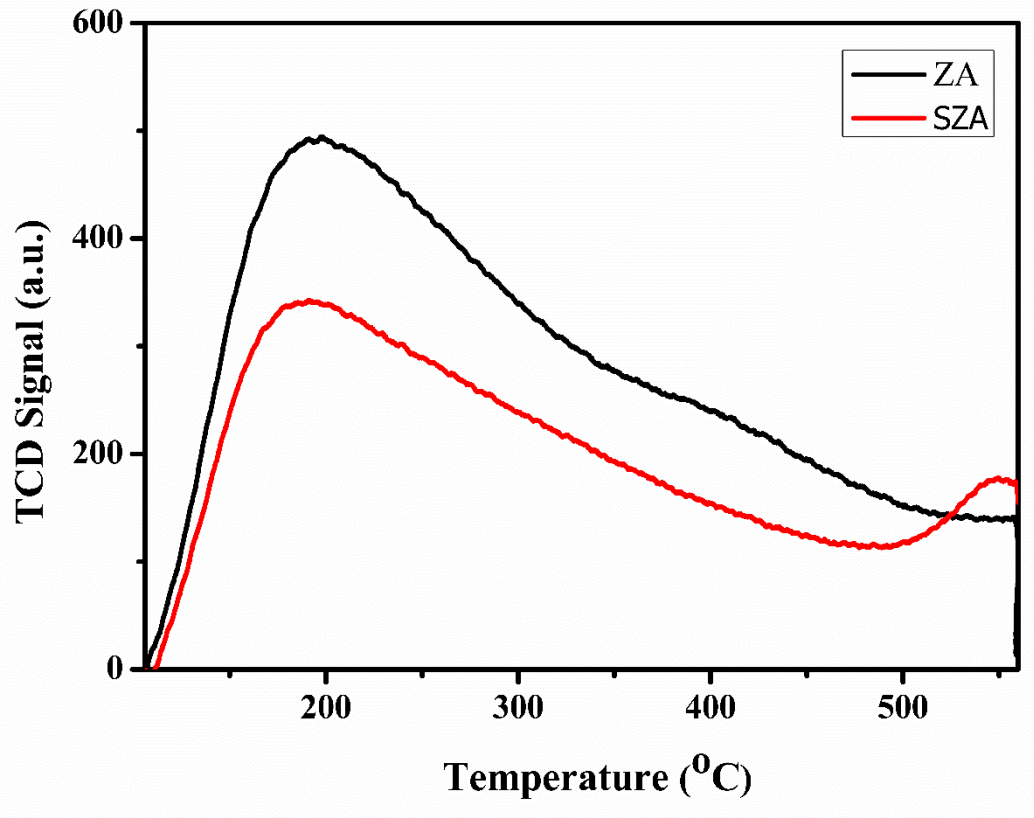

Figure 4.5 NH3-TPD profile of ZA and SZA catalyst

Table. 4.1 Surface properties and amount of acidic sites of the synthesized catalysts

Catalyst	Surface area(m^2/g)[a]	Pore volume (cm^3/g)[b]	Average pore diameter (nm)[c]	Acidic sites (mmol/g)[d]
ZA	20.1	0.07	13.8	0.27
SZA	2.9	0.01	14.7	1.35

[a] The surface area was calculated by BET method.

[b] Pore volume was determined by the amount of nitrogen adsorbed (p/p_0=0.990).

[c] Average pore diameter was determined by using BJH method.

[d] Acidity was determined by NH_3-TPD analysis.

4.3.6. XPS analysis

The XPS analysis of the SZA catalyst was performed, and the obtained graph is depicted in Figure 4.6. The obtained peaks of all elements were calibrated by taking the C 1s peak as a reference. Two characteristic peaks of Zr show the binding energy of Zr $3d_{3/2}$ at 182.3 eV and $3d_{5/2}$ at 184.6 eV, confirming the zirconia present in the IV oxidation state. The peaks at 183.1 and 186.0 eV indicate the presence of Zr (IV) following treatment with H_2SO_4, while the peaks at a binding energy of 183.6 eV correspond to the bridging oxygen between zirconia and alumina metals [95,96]. Al 2p spectra also demonstrate three deconvoluted peaks. The ZrAl-O bonds are observed at a binding energy of 75.8 eV, while other peaks at 75.2 eV may be assigned to the bonding of electron attracting group (such as sulfur) with ZrAl-O. Furthermore, the binding energy at 74.8 eV shows the Al-OH bond. The two different binding energies observed at 169.4 eV and 170.2 eV correspond to the S $2p_{3/2}$ and S $2p_{1/2}$, respectively, indicating the presence of sulfur in the VI oxidation state in S 2p spectra. The higher oxidation state indicates the formation of a bidentate sulfate group on the solid catalyst, suggesting strong acidic sites. Similarly, O 1s spectra show the four deconvoluted peaks. The first peak observed at 532.9 eV is attributed to the Al-OH bond, whereas the second peak at 532.2 eV corresponds to the sulfated oxygen group. The third, at 531.7 eV, is attributed to the bridging oxygen between zirconium and aluminum, while the fourth peak, at 530.6 eV, is associated with the lattice oxygen in the zirconium oxide network [94,97].

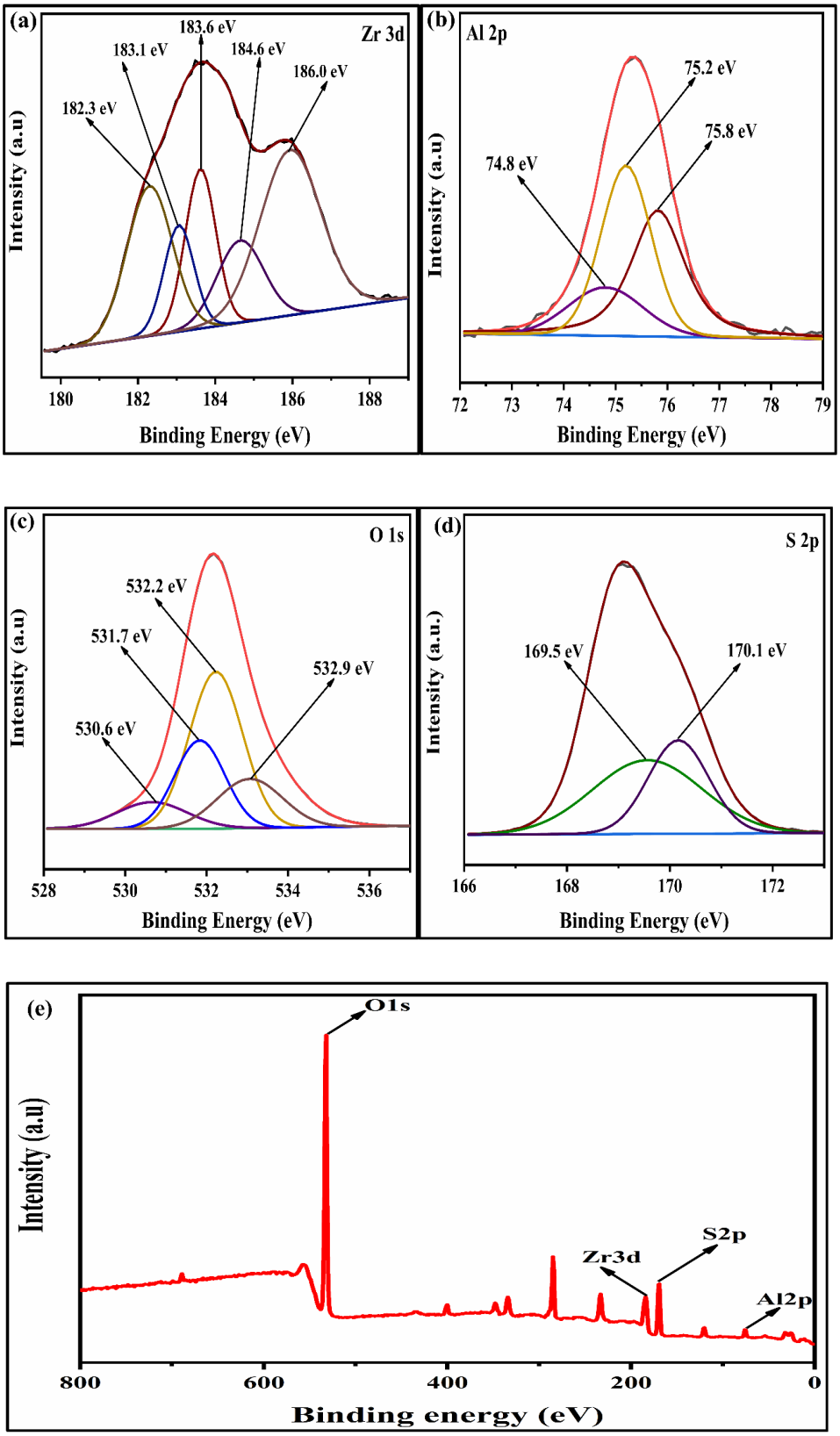

Figure 4.6 XPS spectra of (a) Zr 3d, (b) Al 2p, (c) O1s (d) S2p and (e) survey peak of synthesized SZA catalyst

4.3.7. SEM-EDX analysis

The morphology and elemental composition of the catalyst surface were explored by SEM-EDX images and illustrated in Figure 4.7. Catalyst ZA shows a grain-like structure with variable shape and size, which could be due to the homogeneous mixing of ZrO_2-Al_2O_3, as depicted in Figure 4.7 (a). SZA catalyst shows that the agglomerated irregular grain-like structure might be due to the impregnation of the sulfate group, as shown in Figure 4.7 (b). The reused catalyst in the glycerol acetalization reaction shows the same morphology during the course of the reaction, confirming the catalyst's stability, as presented in Figure 4.7 (c)[98]. The elemental composition of the catalyst was done through energy-dispersive X-ray (EDX) spectroscopy, anticipated the presence of Zr, Al, O, and S is depicted in Figure 4.7 (d) & (e). From the EDX data, it was found that the atomic and weight percentages of Zr and Al are present in high concentrations. However, sulfur content is low on the catalyst surface, affirming the effective impregnation of sulfur into the catalyst and indicating the absence of other contamination on the catalyst's surface.

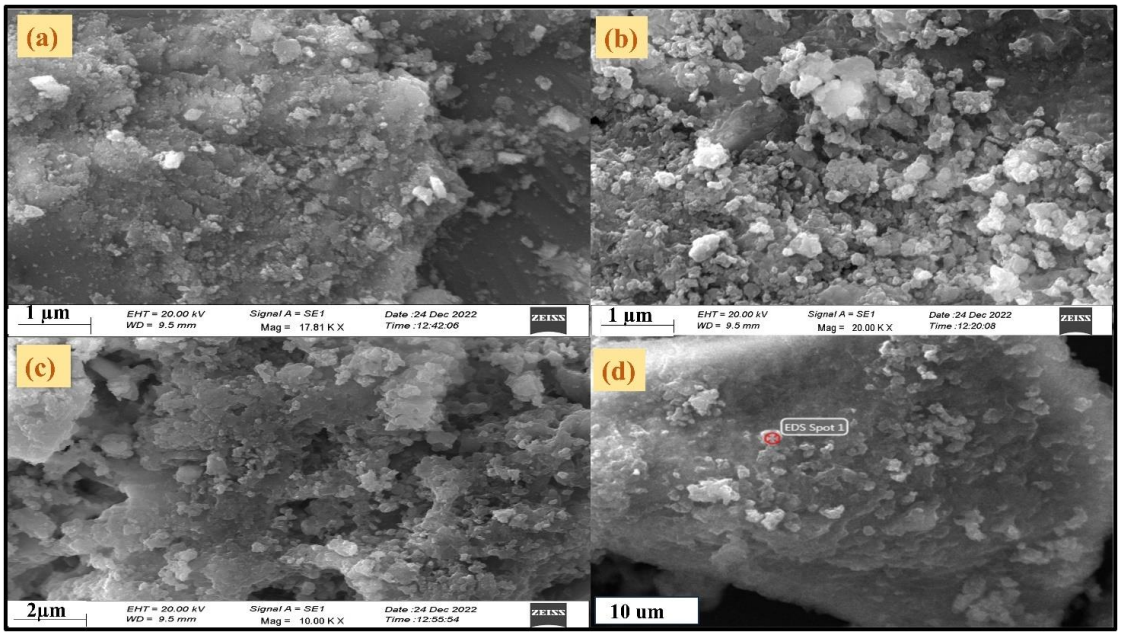

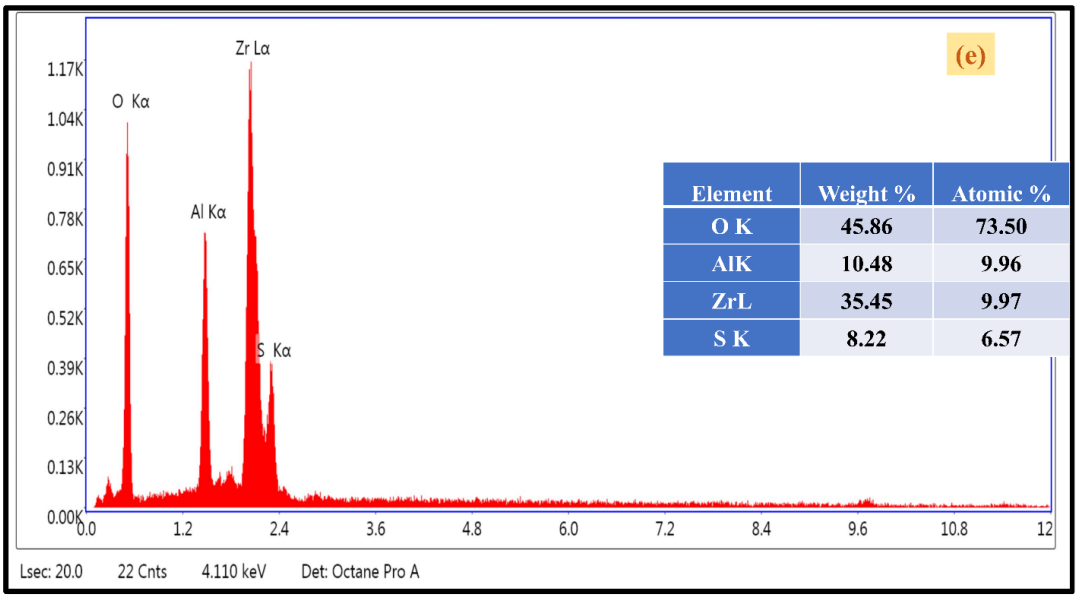

Figure 4.7 FE-SEM image of (a) ZA, (b) SZA calcined at 550 °C, (c) recycle SZA at 550 °C, (d) and (e) EDX spectra of SZA catalyst

4.4 Evaluation of catalyst for solketal synthesis

The glycerol acetalization with acetone was carried out in a 100 ml round bottom flask associated with a reflux condenser. The whole glass tractor setup was immersed in a silica oil bath to provide continuous heating. During the experiment, 21.7 mmol of glycerol and 217 mmol of acetone were taken in a reactor with 3 wt. % of catalyst (with respect to the glycerol) and allow to stir for 180 minutes at 70 °C. After completion of the reaction, the synthesized product was separated by centrifugation. The obtained product mixture was quantitatively analyzed by GC-MS. Besides GC-MS, ^{1}H & ^{13}C NMR and FTIR were also performed to confirm the synthesized product. All the synthesized catalysts were applied for solketal synthesis and its conversion and selectivity, as represented in Table 4.2.

Table 4.2 Catalyst screening for solketal synthesis with time

Catalyst	Conversion (%)[a]	Solketal selectivity (%)[a]	TOF (mol g^{-1} h^{-1})[b]

ZA	22	75	0.02
SZA	99.2	98.9	0.12

[a] Conversion of glycerol was calculated by using GC-MS analysis.

[b] TOF (mol $g^{-1}h^{-1}$) calculated by the moles of glycerol converted per gram of catalyst per hour.

4.4.1. Characterization of the synthesized product

4.4.1.1. ^{1}H and ^{13}C NMR

The NMR spectra of the synthesized product are illustrated in Figure 4.8. After completion of the acetalization reaction, the product mixture was separated and underwent ^{1}H as well as ^{13}C NMR using the Bruker 500 MHz spectrometer. DMSO-d6 is used as an NMR solvent. Figure 4.8 (a) shows the proton NMR spectra of the synthesized product, which has various types of multiplet peaks at different chemical shift values. The two singlet peaks at 1.26 and 1.30 ppm chemical shift values responsible for the six-methyl hydrogen and a broad single peak of the hydroxyl group present at 2.0 ppm. The chemical shift value observed at 3.37-4.79 ppm corresponds to the multiplet peak of -CH and $-CH_2$ groups, confirming the transformation of glycerol to solketal. Figure 4.8 (b) shows the ^{13}C NMR spectra of solketal, and it was found that two methyl carbon peaks of cyclic solketal were found at 25.73 and 27.08 ppm. The peaks present at 76.59 ppm are responsible for the $-CH_2-CH-CH_2-$ carbons of a ring, while the other peaks are observed at 66.40 ppm and 63.46 ppm for two $-CH_2$ carbon of solketal. The peak was found at 108.68 ppm, corresponding to the most deshielded peak of ketal carbon that confirms the formation of five-membered solketal. The deuterated multiplet dimethyl sulfoxide solvent peak was observed at 39.65 ppm [99].

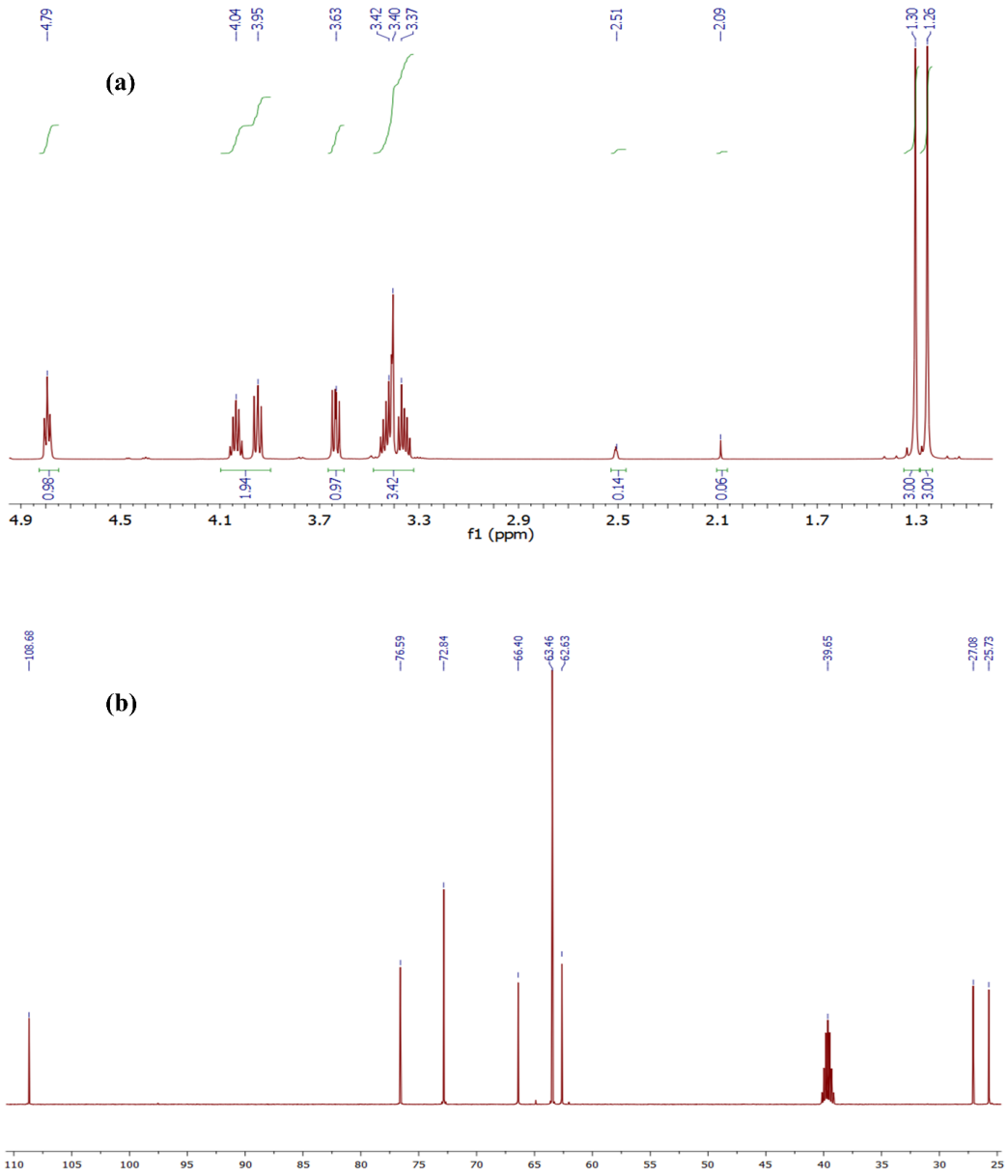

Figure 4.8 (a) ^{1}H NMR spectra (b) ^{13}C spectra of synthesized product

4.4.1.2 GCMS studies of the synthesized product

After completion of the reaction, the synthesized product can be evident through gas chromatography-mass spectroscopy (GC-MS), shown in Figure 4.9 The product peak was observed at 3.929 and 4.193 min. showed the presence of five-member ring solketal and six-member ring acetal. The peak appeared at 4.845 min. indicates the remaining small amount of unconverted glycerol.

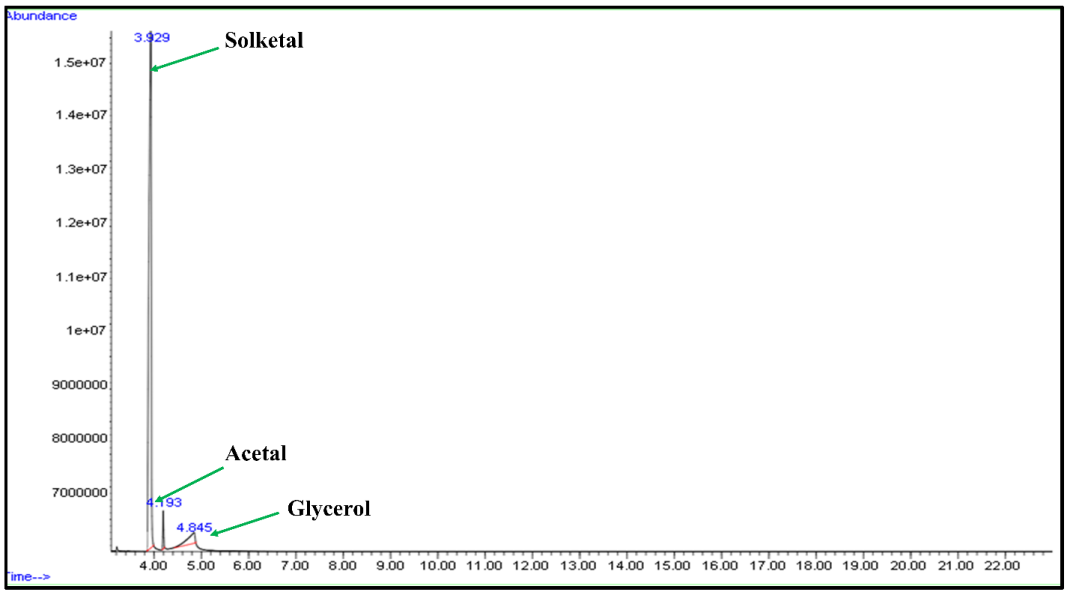

Figure 4.9 GCMS spectra of synthesized product

4.4.1.3. FTIR spectra of glycerol, synthesized product, and standard solketal

Further verification of the synthesized product was performed by FTIR analysis. The synthesized product was confirmed by comparing the characteristic peaks with commercially available solketal, which confirms the formation of solketal from glycerol. The FTIR spectra of glycerol-synthesized solketal and standard solketal are shown in Figure 4.10. Figure 4.10 (a) illustrates the FTIR of glycerol. The absorption peak found at ~3335 cm^{-1} shows the stretching of the -OH group. The -C-H stretching peak of glycerol is present in the absorption range of 2884-1936 cm^{-1}. Other peaks at 1414 cm^{-1} correspond to the bending vibration of the C-OH group. Additionally, a peak closer to the bending vibration of the -OH group within the -C-OH group, ~ 1109 cm^{-1}, is regarded as the C-O stretching peak of 1^{o} alcohol. Furthermore, a peak at 920 cm^{-1} signifies the bending vibration of the -OH group in glycerol moiety [100,101].

FTIR spectra of both synthesized and standard solketal are depicted in Figure 4.10 (b) and (c). It was evident that both synthesized and standard solketal showed the same characteristic peaks. In synthesized solketal, the stretching peaks around ~ 3435 cm^{-1} are

attributed to the -OH group in cyclic solketal. The intensity of this peak is found to be reduced compared to glycerol, indicating the conversion of glycerol to solketal. The C-H stretching frequency of the methyl group was observed within the range of 2885-2984 cm^{-1}. The absorption peak at 1380 cm^{-1} indicates the "umbrella" movement of the methyl group in the cyclic ring. Another peak at 1216 cm^{-1} is assigned to the -C-O bond of the dioxolane ring. The characteristic absorption peaks present at 1216 and 1156 cm^{-1} are attributed to the asymmetric vibration of -C-O-C-O-C- bonds, while bands at 922 and 792 cm^{-1} correspond to the same bond in the solketal ring. Another peak found at 1045 cm^{-1} is attributed to the -C-C-OH stretching of the alcoholic group in the 4^{th} position present in cyclic solketal. Several characteristic peaks, such as 1045, 1156, 1216, and 1380 cm^{-1}, are absent in synthesized solketal, indicating the conversion of glycerol into solketal [101].

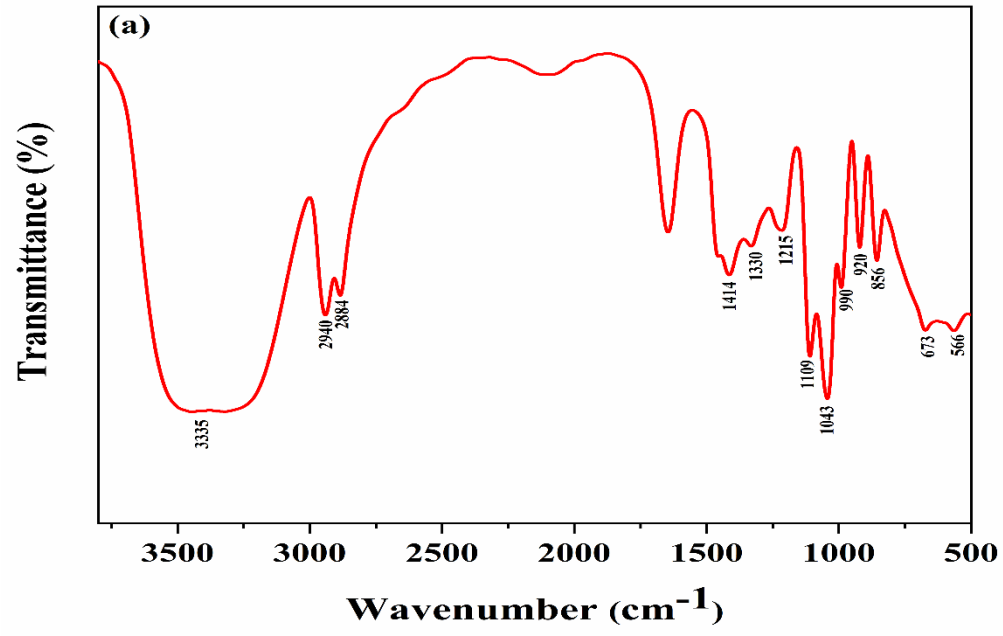

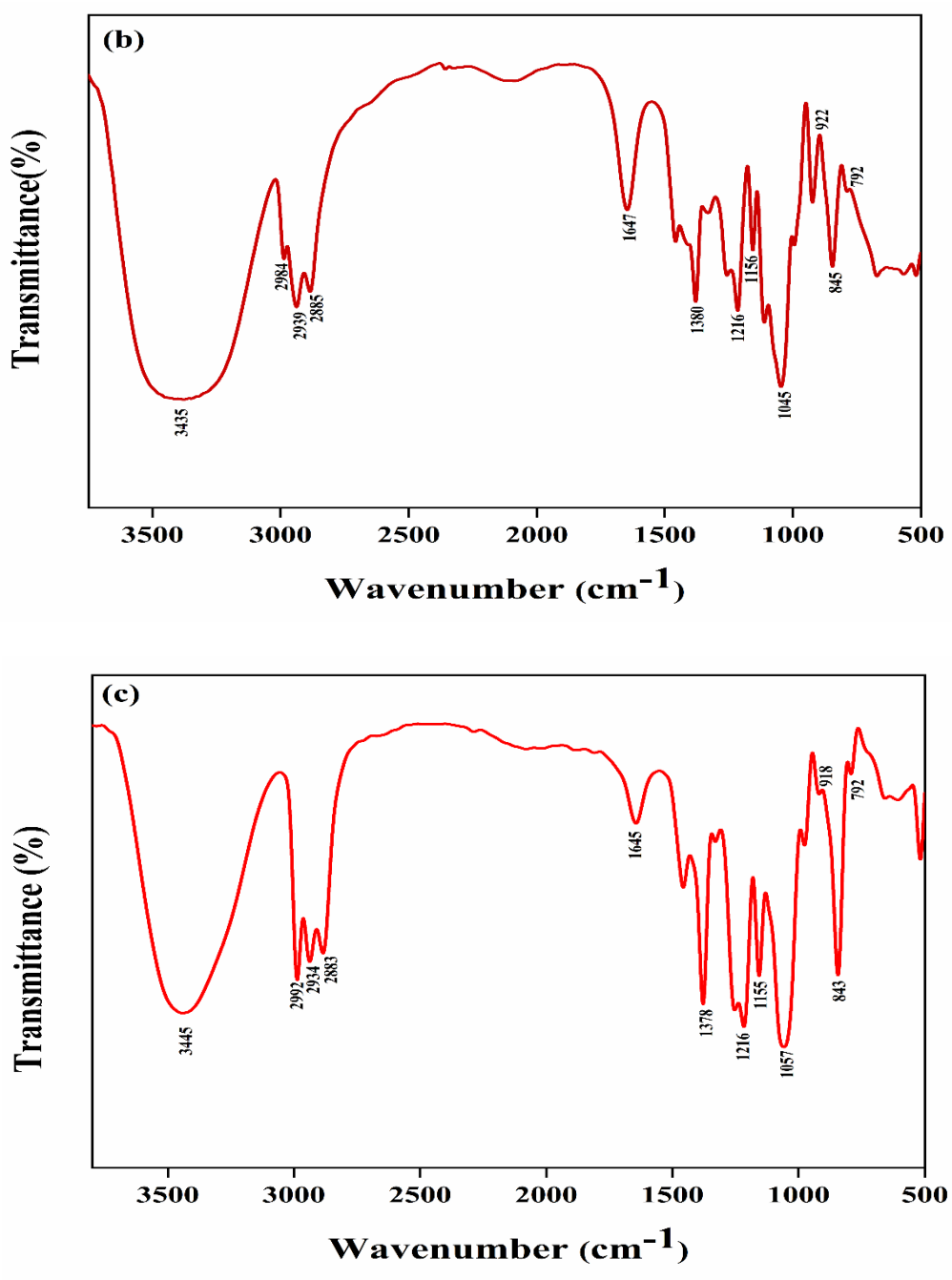

Figure 4.10 FTIR spectra of (a) glycerol, (b) synthesized product, and (c) standard solketal

4.5 Proposed reaction mechanism in glycerol acetalization reaction

The acetalization reaction of glycerol with acetone follows the Langmuir-Hinshelwood (LH) mechanism. This reaction mechanism proceeds in various steps, as illustrated in Figure 4.11. Initially, glycerol and acetone molecules diffused onto the catalyst's surface

and become adsorbed on the catalyst pores. The first step involves the protonation of the carbonyl group with the acidic proton of the SZA catalyst, enhancing the electrophilicity of carbonyl carbon. Subsequently, in the second step, the lone pair of the -OH group of glycerol acts as a nucleophile, attacking the electrophilic carbon of the carbonyl group. The third step involves deprotonation with the formation of the hemiacetal intermediate. This intermediate, being highly unstable, undergoes cyclization, accompanied by the elimination of water molecules by the SN_2 nucleophilic substation reaction through two pathways. A five-membered solketal is produced when 2^o -OH of glycerol attacks the tertiary carbon of the intermediate. On the other hand, if the 1^o -OH group attacks, the tertiary carbon leads to the cyclization of a six-member acetal. However, the formation of a five-member solketal is kinetically more favorable over the six-member acetal; as a result, this reaction predominates the production of solketal [102].

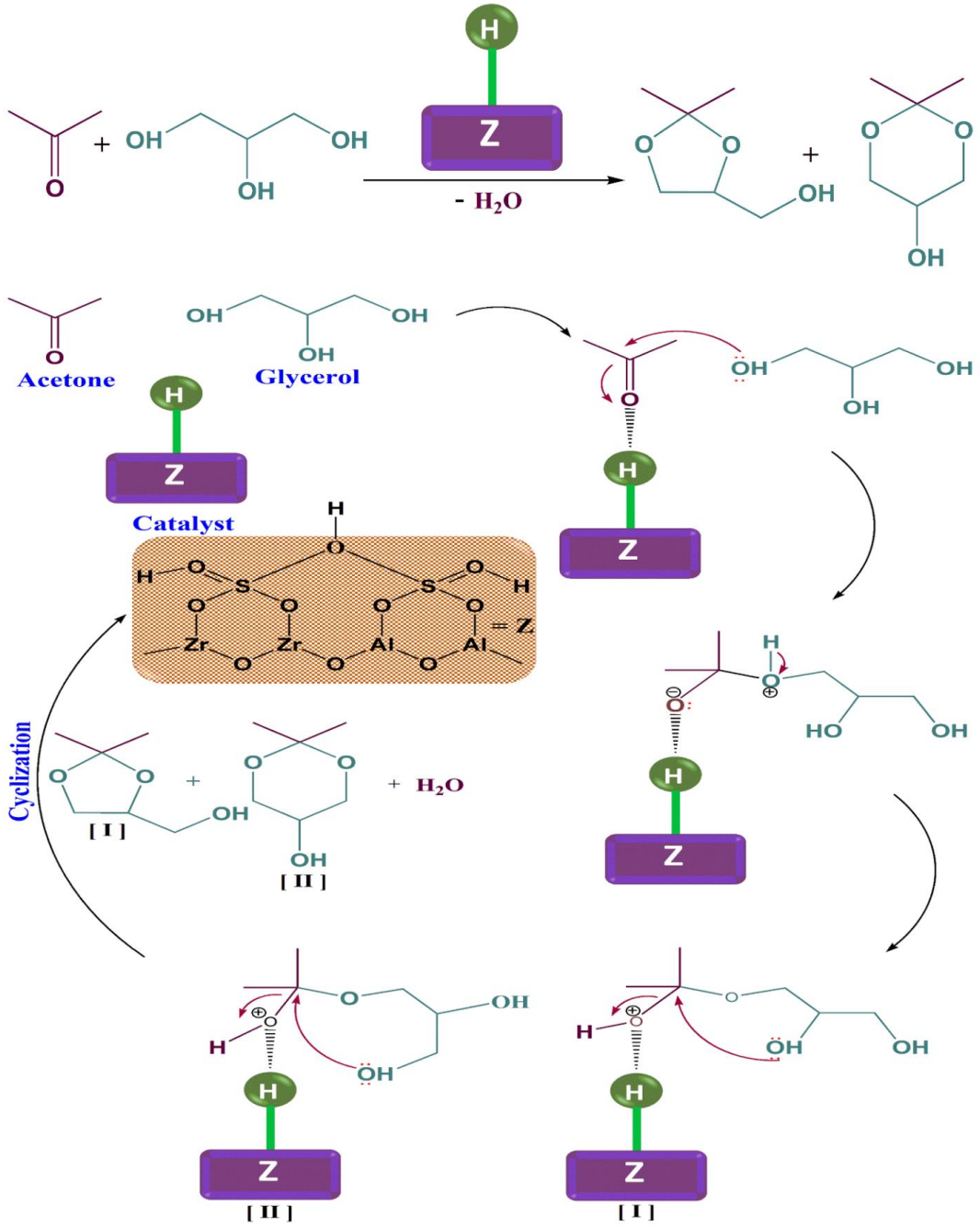

Figure 4.11 Plausible reaction mechanism for acetalization reaction of glycerol with acetone using SZA catalyst

4.6 Optimization of reaction parameters in glycerol acetalization

Various reaction-affecting parameters like the molar ratio of glycerol and acetone, reaction time, reaction temperature, and catalyst weight percentage that affected the

acetalization of glycerol were studied, and the obtained outcomes were elucidated below.

4.6.1. Effect of glycerol to acetone molar ratio

In the glycerol acetalization reaction, the effect of glycerol to acetone molar ratio was optimized while keeping all other reaction parameters constant (i.e., time = 180 min, T = 70 ^{o}C, catalyst loading = 3 wt. %), shown in Figure 4.12 (a). As the glycerol to acetone molar ratio varied from 1:2 to 1:10, a notable increase in glycerol conversion and solketal yield was observed, reaching up to 99.2 % and 98.1 %, respectively. Consequently, the selectivity of solketal is high at 98.9 % compared to ketal. Moreover, with an increase of glycerol to acetone molar ratio from 1:15 to 1:20, a small change was found in glycerol conversion, reaching up to 99.4 % and 99.6 %, respectively. This increase in glycerol conversion may be attributed to the enhanced accessibility of glycerol to acetone, which increases the equilibrium toward the product formation, promoting the product formation. This outcome indicates that minimal changes in glycerol conversion were observed when the glycerol-to-acetone molar ratio was increased [103].

4.6.2. Effect of reaction time

The impact of reaction time on glycerol acetalization is another crucial factor that affects both the conversion and yield percentage of solketal. In this study, reaction time was varied while maintaining all other reaction parameters at optimized conditions, as shown in Figure 4.12 (b). It was found that on the increase in reaction time from 60 min to 180 min, a notable conversion in glycerol was observed, rising from 63 % to 99.2 %, along with an increase in solketal yield up to 98.1 %. This observation could be observed due to the augmentation of a number of reacting molecules, facilitating the formation of new bonds following the cleavage of pre-existing ones. However, beyond 180 minutes, a decline in conversion was found. This decrease could be attributed to the hydrolysis of the product facilitated by the formation of water during the prolonged reaction duration

[104,105].

4.6.3. Effect of reaction temperature

Temperature is another crucial variable impacting glycerol acetalization reaction. In this study, the catalytic experiment was explored by varying the temperature from 50 ^{o}C to 90 ^{o}C while maintaining other factors at optimized reaction conditions, as shown in Figure 4.12 (c). It was found that at lower temperatures, 40 ^{o}C to 50 ^{o}C, both glycerol conversion and yield percentage of solketal are low, i.e., 64 % and 61 %, respectively. However, as the temperature rose to 70 ^{o}C, the conversion reached 99.2 %. This suggests that the higher reaction temperature provides a sufficient amount of kinetic energy to the reactant molecules, facilitating effective glycerol conversion. Beyond 70 ^{o}C, both glycerol conversion and solketal yield declined due to the acetone evaporation. As a result, glycerol acetalization is hindered by a reduction in its availability in the reaction mixture. Since acetalization is an exothermic process, excessively high temperatures are unnecessary for glycerol conversion [105]. Thus, the optimum temperature for this reaction was found to be 70 ^{o}C.

4.6.4. Effect of catalyst weight percentage

The impact of catalyst weight percentage on glycerol acetalization was investigated by adjusting the catalyst concentration. Figure 4.12 (d) illustrates the conversion and yield percentage of solketal. It is evident that no glycerol conversion was observed in the absence of a catalyst. On increasing the catalyst concentration from 0.5 wt. % to 3.0 wt. %, a gradual conversion in glycerol is observed, ranging from 68 % to 99.2 %. This increase in glycerol conversion and solketal yield can be attributed to the augmented number of accessible active sites on the catalyst's acidic surface, facilitating enhanced interaction and collision among the reacting molecules. However, beyond a 3 wt. % of catalyst amount, the overall glycerol conversion decreased due to hydrolysis of the

product [106,107]. Consequently, the optimal catalyst weight percentage for glycerol conversion was determined to be 3 wt. %.

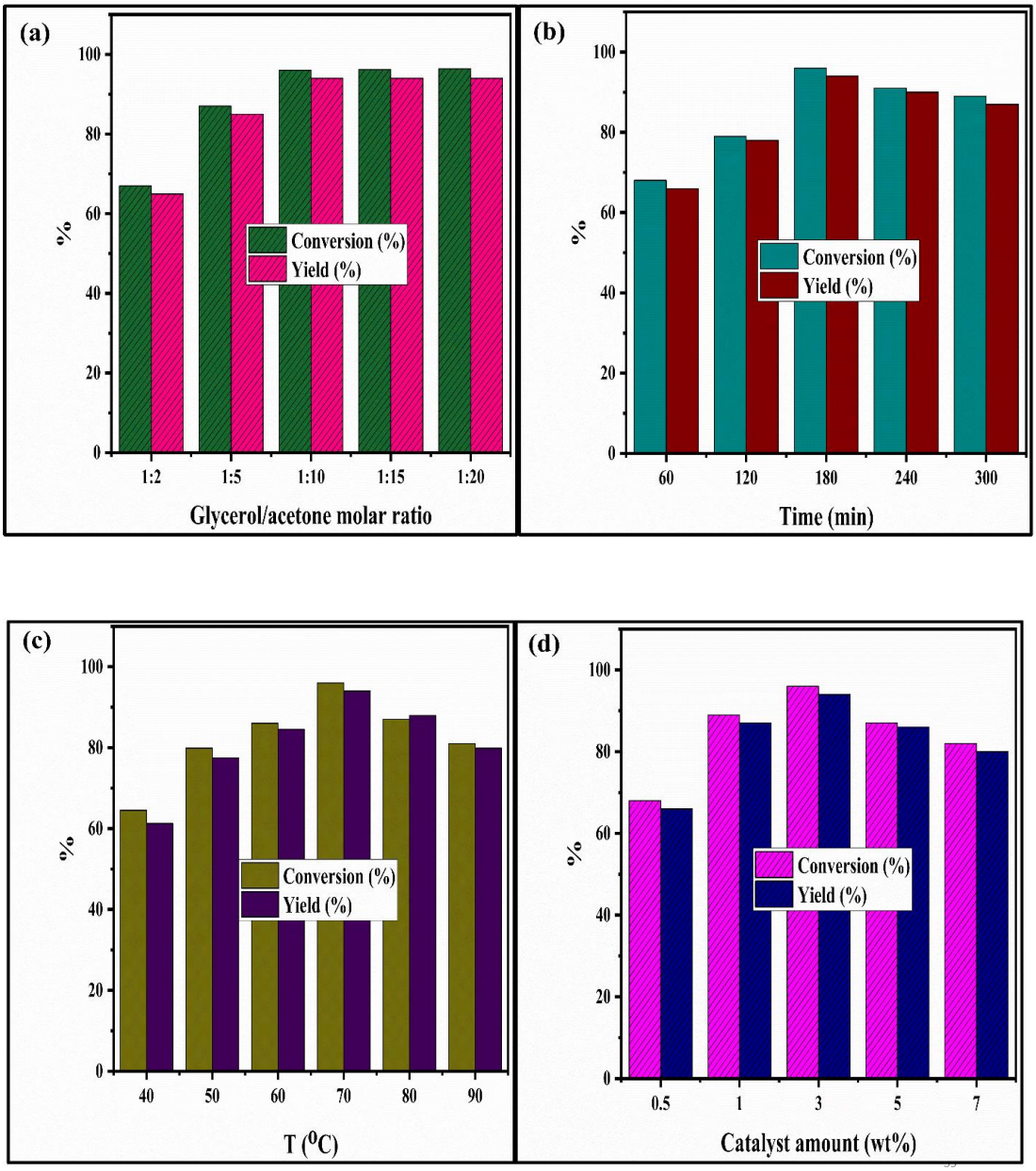

Figure 4.12. Effect of reaction parameters on acetalization (a) Glycerol/acetone molar ratio (reaction temperature =70 °C, reaction time 180 min, catalyst amount = 3wt.% with respect to glycerol used) (b) Reaction time (reaction temperature = 70 °C, 1:10, catalyst amount = 3 wt.%) (c) Reaction temperature (1:10, catalyst amount

= 3 wt.%, reaction time = 180 min) (d) Catalyst amount (1:10, reaction temperature = 70 °C, reaction time = 180 min)

4.7 Green metrics study of glycerol acetalization

The environmental impact of solketal synthesis employing SZA catalysts was investigated by examining various green parameters such as the Environmental factor (E-factor) and Process Mass Intensity (PMI). These parameters serve as an indicator of the eco-friendliness nature of the synthesized catalysts utilized in solketal synthesis. The E-factor is quantified as the ratio of the total waste generated to the desired product. A higher E-factor indicates a higher amount of waste generated during the process, thus exerting a negative environmental impact.

$$\text{E-factor} = \frac{Total\ waste\ generated\ (mg)}{desired\ product\ (mg)} \quad (4.1)$$

Thus, for calculating the E-factor, glycerol, acetone, catalyst amount, and the resulting product were taken into consideration. Water is generated as a by-product during solketal synthesis, typically benign and potentially useful as a solvent in various chemical syntheses, thus not classified as waste. Subsequently, an excess amount of acetone was recovered from the erection mixture using a rotatory evaporator for further acetalization reaction and was also excluded from the waste calculation. The calculated value of the E-factor for solketal synthesis was found to be 0.083, falling within the range of 0-1, indicating minimal waste generation throughout the process. PMI serves as another environmental measure employed to evaluate the sustainability of solketal synthesis. It takes into account the overall quantity of components utilized in the reaction matrix, including reactants, reagents, catalysts, and solvents.

$$\text{PMI} = \frac{Total\ mass\ of\ material\ used\ in\ acetalization\ process\ (mg)}{Mass\ of\ isloted\ product\ (mg)} \quad (4.2)$$

In this process, the acetalization reaction is operated in solvent-free conditions, relying

on the quantities of catalyst, glycerol, and acetone. Similarly, for PMI calculation, any surplus acetone was recovered and subsequently reused in solketal synthesis. The resultant PMI value for solketal synthesis was found to be 1.87 mg. Such a green metrics study indicates minimal waste generation and an environmentally friendly nature of the process [107].

4.8 Reusability study of SZA catalyst

The catalyst's reusability plays an important role in evaluating its stability and catalytic effectiveness. Following each catalytic experiment, the spent catalyst was separated from the reaction mixture through centrifugation. Subsequently, it was washed 3-4 times with ethanol to eliminate impurities adhered to its surface for further application. The obtained catalyst was then dried for 5 h at 80 ^{o}C in an oven to facilitate glycerol acetalization under the same optimized reaction conditions. The obtained result of the recycled catalyst is illustrated in Figure 4.13. The catalyst displayed remarkable catalytic activity, achieving > 90 % glycerol conversion for the first three cycles with negligible activity loss. However, a decline in glycerol conversion was found in the 4th and 5th reuse cycles, dropping from 87 % to 81.8 %, respectively. This decrease in catalytic activity is likely attributed to the mass loss during the recycling process, indicating potential leaching of the surface sulfate group, leading to decreased catalytic efficiency. To investigate the reason behind the loss, a leaching test was conducted using a hot filtration method. 0.14 g of catalyst was mixed with 37 ml of acetone in a round bottom flask and stirred for 2 h at 70 ^{o}C. Afterward, the catalyst was separated, and 3.6 ml of glycerol was added to the filtrate for further reaction under the same conditions. The conversion percentage of glycerol and solketal yield was calculated and compared with the uncatalyzed experiment shown in Figure 4.14. It was found that the catalyst was present in minimal amounts in the filtrate. XRD and FTIR analysis of the reused catalyst exhibits a similar pattern to the

fresh catalyst shown in Figure. 4.15 and Figure 4.3, indicating the structural integrating retention. Similarly, the SEM analysis of the reused catalyst exhibits a morphology similar to that of the fresh catalyst in Fig 4.7 (c).

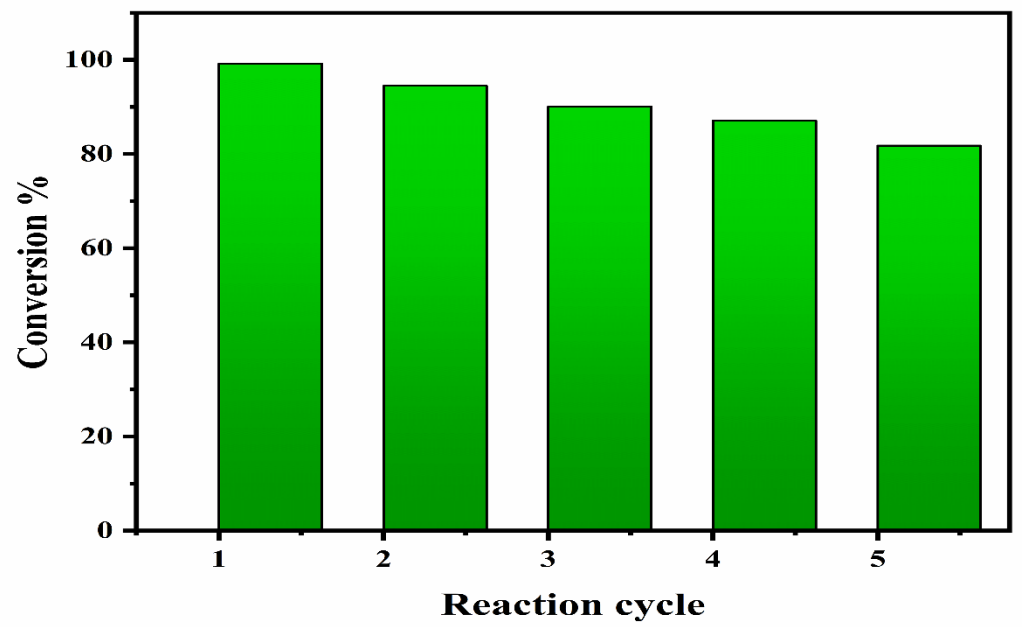

Figure 4.13 Reusability test of synthesized SZA catalyst in acetalization reaction

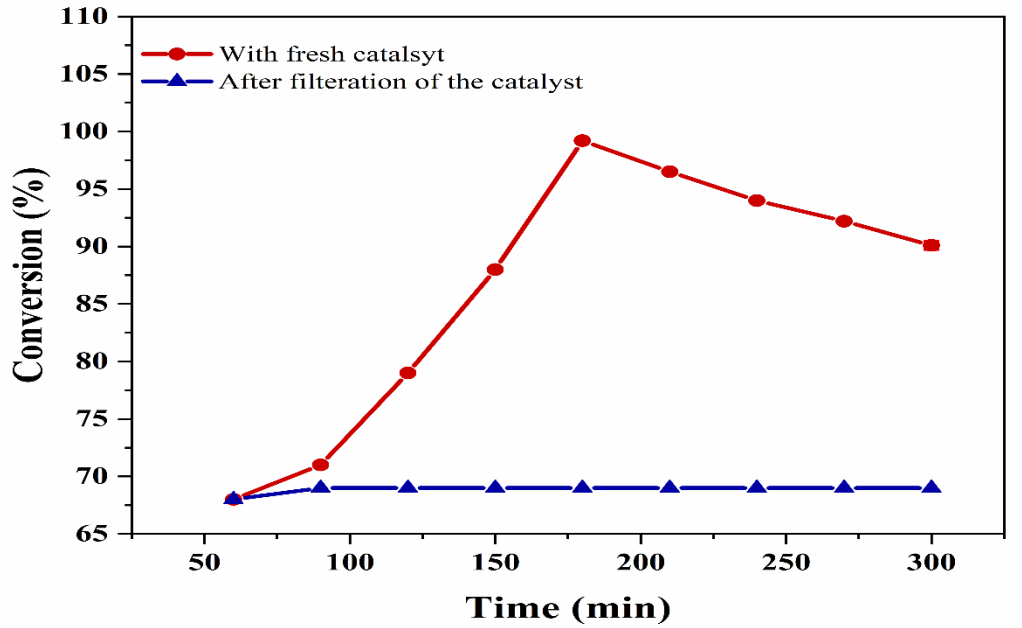

Figure 4.14 Heterogenous nature of SZA catalyst

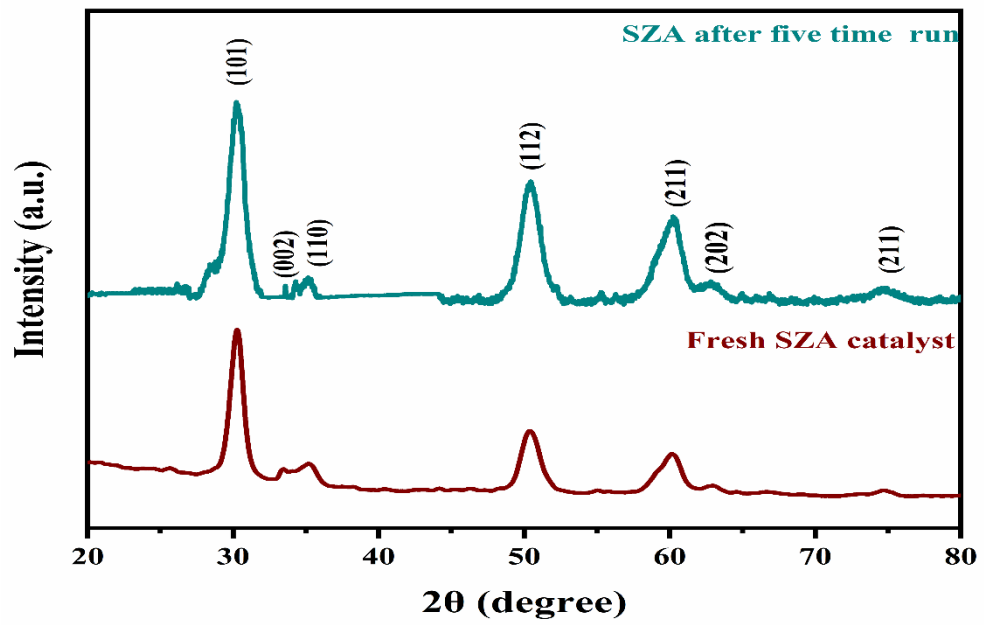

Figure 4.15 XRD image of reused SZA catalyst

4.9 Comparison of synthesized SZA catalytic activity with previously reported catalysts

The synthesized catalyst's catalytic activity, reusability, and efficiency in acetalization were compared with those of previously reported catalysts, as presented in Table 4.3. Previously, zirconia-based catalysts, such as Zr-S-400 [108] and ZrP-200 [109], exhibited significant catalytic activity, but their glycerol conversion was low. MoO_3/SiO_2 [110,111] and Zr-TUD-1, Hf-TUD-1, and Sn-MCM-15 [111] demonstrated poor catalytic activity, requiring long reaction time, high temperature, and resulting in low glycerol conversion, and reusable up to 4th traction cycle. Similarly, $Co[II](Co[III]_xAl_{2-x})O_4$ [105] yielded very low glycerol conversion at the high reaction temperatures. PSF polymer [109,112] achieved a remarkable conversion of 97 % glycerol with a 95 % yield in the presence of prolonged reaction time. Similarly, Zeolite (BEA, MFI, FAU) [112] and Algerian acid-activated clays [113] found appreciable glycerol conversion but needed longer reaction time. Montmorillonite [110,114], although it shows a 54 % glycerol conversion in a short

reaction time, catalysts have poor recyclability and are reusable only for three catalytic cycles. Moreover, catalysts like MoO_3/SiO_2 and Montmorillonite required toluene and CH_3CN as solvents for higher glycerol conversion [110]. Although $Fe(NO_3)_3.9H_2O$ required excess acetone for higher glycerol conversion, it remained stable up to the 3rd reaction cycle [115]. Similarly, other reported catalysts like H-Beta Zeolite [116], WO_x/MCM-41[106], and 1Nb:0.05Al exhibit relatively lower catalytic activity in prospects of Gly: ace molar ratio, reaction time and temperature, poor reusability, and low conversion. To tackle the challenges associated with the aforementioned catalyst, we synthesized SO_4^{-2}/ZrO_2-Al_2O_3 catalysts to facilitate a more straightforward, efficient, and solvent-free process for enhancing glycerol acetalization reaction. Delightfully, the synthesized catalyst achieved a remarkable 99.2 % glycerol conversion with 98.9 % selectivity towards a fine-member solketal under mild reaction conditions. Furthermore, the catalyst exhibited consistent catalytic activity throughout the reaction, demonstrating stability and excellent reusability for up to 5th catalytic cycle, thus making it more comparable to other reported catalysts.

Table. 4.3 Comparative study of synthesized SZA catalyst with previously reported catalysts for solketal synthesis.

Catalyst	Catalyst loading	Reaction time (min)	Reaction temperature (^oC)	Gly: Ace molar ratio	Solvent	Glycerol conversion (%)	Endurance capacity	Ref.
Zr-S	0.3 (wt. %)	60	40	1:6	free	80	4th reaction cycle	[26]
ZrP-200	5 (wt. %)	180	50	1:10	free	85.7	5th reaction cycle	[52]

PSF polymer	8 (wt. %)	300	60	1:5	free	97	4^{th} reaction cycle	[53]
Co[II](Co[III]$_x$Al$_{2-x}$)O$_4$	5 (wt. %)	180	130	1:10	free	69.2	5^{th} reaction cycle	[45]
1Nb:0.05Al	2.7 (wt. %)	360	50	1:4	free	84	4^{th} reaction cycle	[54]
WO_x/MCM-41	10 (wt. %)	120	50	1:6	free	78.52	4^{th} reaction cycle	[55]
$Fe(NO_3)_3.9H_2O$	0.3 (mol %)	60	60	1:20	free	90	3^{rd} reaction cycle	[56]
H-Beta Zeolite	5 (wt. %)	60	28	1:2	free	86	Not reported	[57]
Hf-TUD-1	3 (wt. %)	360	80	1:1	free	65	4^{th} reaction cycle	[58]
Zr-TUD-1	3 (wt. %)	360	80	1:1	free	64	4^{th} reaction cycle	[58]
Sn-MCM-1	3 (wt. %)	360	80	1:1	free	62	4^{th} reaction cycle	[58]
MoM_3/SiO_2	10 (wt. %)	480	100	1:1(benzaldehyde)	Toluene	72	Not reported	[59]
Montmorillonite	0.7 (wt. %)	30	50	1:4.1	Free	54	3^{rd} reaction cycle	[60]
Montmorillonite	0.7 (wt. %)	30	50	1:4.1	CH_3CN	94	3^{rd} reaction cycle	[60]
Zeolites (BEA, MFI, FAU)	6 (wt. %)	480	50	1:3	Methanol	85	Not reported	[61]
Algerian acid-activated	5 (wt. %)	2,880	40	1:4	free	89	Not reported	[62]

clays							
SZA (Present work)	3 (wt. %)	180	70	1:10	free	99.2	5^{th} reaction cycle

5. Conclusions

In this study, a heterogeneous acid SZA catalyst was synthesized through coprecipitation, followed by a wetness impregnation process. The coprecipitation process yielded a tetragonal ZA phase, while the subsequent wetness impregnation process allowed the production of an active acidic phase of the catalyst. This designed catalyst was employed in solketal production using an acetalization reaction of acetone with bio-waste glycerol obtained from biodiesel production. The catalyst's high activity depends on its acidity, which significantly influences the glycerol conversion and yield of solketal. Several characterization techniques, including TGA, XRD, FTIR, BET-surface area, SEM-EDX, XPS, and NH_3-TPD, revealed that impregnation of sulfur on the ZA lattice enhanced the catalyst's acidity. All these characterization techniques proved that SZA catalysts enhance glycerol conversion. The quantitative and qualitative analysis of the synthesized product was also performed using ^{1}H, ^{13}C NMR, FTIR, and GCMS analysis. The glycerol conversion and solketal yield percentage depended upon the catalyst's acidity and reaction conditions. The SZA catalyst exhibited a higher turnover frequency (TOF) of 0.12 ($molg^{-1}h^{-1}$), indicating robust catalytic activity in glycerol acetalization reaction. The excellent solketal yield was also optimized by varying the reaction parameters and obtained at optimized conditions. Moreover, green metrics parameters like E-factor and PMI demonstrated that both SZA catalyst synthesis and solketal production process are environmentally benign and eco-friendly in nature. Overall, the synthesized SZA catalyst proves to be cost-effective and highly efficient for acetalization and is recyclable for up

to 5th catalytic cycle. Its further application in glycerol acetalization could enhance the economic feasibility and cost-effectiveness. Its potential application on an industrial scale for solketal synthesis could establish the sustainability of the market.